Journal of Power Sources 520 (2022) 230896

Contents lists available at ScienceDirect

Journal of Power Sources

journal homepage: www.elsevier.com/locate/jpowsour

Photo and thermal crosslinked poly(vinyl alcohol)-based nanofiber membrane for flexible gel polymer electrolyte

Nazym Kassenova [a,b], Sandugash Kalybekkyzy [a,b,**], Memet Vezir Kahraman [c], Almagul Mentbayeva [a,b,*], Zhumabay Bakenov [a,b]

[a] Department of Chemical and Materials Engineering, School of Engineering and Digital Sciences, Nazarbayev University, Kabanbay Batyr Ave. 53, Nur-Sultan, 010000, Kazakhstan
[b] National Laboratory Astana, Nazarbayev University, Kabanbay Batyr Ave. 53, Nur-Sultan, 010000, Kazakhstan
[c] Department of Chemistry, Marmara University, Istanbul, 34722, Turkey

HIGHLIGHTS

- Dual crosslinked gel polymer electrolyte is fabricated by UV-electrospinning method.
- High liquid retention ability was achieved by the unique structure of membranes.
- GPE exhibits high ionic conductivity and mechanical stability.
- Li/$LiFePO_4$ cell with GPE showed excellent electrochemical performance.
- Li dendrite was suppressed with the use of GPE.

ARTICLE INFO

Keywords:
Gel polymer electrolyte
Electrospinning
UV-crosslinking
Maleated polyvinyl alcohol
Tetraethyl orthosilicate
Lithium-ion battery

ABSTRACT

Novel dual crosslinked nanofibrous membranes (DCNMs) were fabricated by a combination of UV-photocrosslinking and thermal sol-gel crosslinking procedures and used as a matrix for gel polymer electrolytes for lithium-ion batteries (LIBs). Flexible nanofibrous membranes were obtained from the solution of poly (vinyl alcohol) (PVA), maleated PVA (PVA-MA), polyethylene glycol diacrylate (PEGDA), and tetraethyl orthosilicate (TEOS) by electrospinning technique. As a matrix for gel polymer electrolyte (GPE), it showed significantly higher ionic conductivity of 1.98×10^{-3} S cm^{-1} than the commercial separators and pure PVDF based GPE. Incorporation of TEOS into the membrane composition, and formation of siloxane bonds (Si–O–Si) greatly increased the conductivity providing excellent mechanical and thermal stability. The assembled lithium metal cell with $LiFePO_4$ cathode exhibited excellent cycling performance and delivered a high reversible capacity of 133 mA h g^{-1} at 0.1 C and retained 87% of the initial discharge capacity after 150 cycles with a stable coulombic efficiency near 100%. The GPE could substantially suppressed the growth of Li dendrites during the stably cycles up to 1000 h, while the cell with the commercial separator failed within 800 h. In consequence, this novel DCNM possesses a potential for application in flexible and safe Li-ion and Li-metal batteries.

1. Introduction

Lithium-ion batteries (LIBs), which currently offer the longest cycle life and highest energy density among secondary batteries, are widely used in various portable devices and electric vehicles [1,2]. However, commercially available LIBs with liquid electrolytes have severe drawbacks related to a liquid solvent such as its volatility, flammability, and leakage, which cause safety problems limiting their application in flexible and wearable electronic devices, especially at elevated temperatures [3]. The alternative Li-ion conducting materials such as polymers,

* Corresponding author. Department of Chemical and Materials Engineering, School of Engineering and Digital Sciences, Nazarbayev University, Kabanbay Batyr Ave. 53, Nur-Sultan, 010000, Kazakhstan.
** Corresponding author. Department of Chemical and Materials Engineering, School of Engineering and Digital Sciences, Nazarbayev University, Kabanbay Batyr Ave. 53, Nur-Sultan, 010000, Kazakhstan.
E-mail addresses: sandugash.kalybekkyzy@nu.edu.kz (S. Kalybekkyzy), almagul.mentbayeva@nu.edu.kz (A. Mentbayeva).

https://doi.org/10.1016/j.jpowsour.2021.230896
Received 18 September 2021; Received in revised form 18 November 2021; Accepted 8 December 2021
Available online 14 December 2021

ceramics, ionic liquids, hybrid films, and electrolyte additives are being developed to overcome the mentioned safety limitations [4]. Replacing a liquid electrolyte with solvent-free alternatives is a promising approach, which became a subject of extensive research in the past few years. Such electrolytes can be categorized as inorganic and polymer-based solid electrolytes (SEs) [5]. Poor interfacial compatibility with electrode materials and their fragility slow down the progress in development of inorganic SEs. In comparison with inorganic SEs, solid polymer electrolytes are more advantageous and promising with their good flexibility and compatibility with electrodes, a wide range of electrochemical stability, and high thermal and mechanical stability [6]. However, low lithium-ion conductivity (10^{-7}-10^{-5} S cm^{-1}) at ambient temperatures is the main drawback of such electrolytes.

Alternatively, gel polymer electrolytes (GPEs) consisting of polymer networks swollen with liquid electrolyte combine privileges of both liquid and solid electrolyte, having high ionic conductivity, good interfacial properties, flexibility, and reduced leakage of liquid electrolyte [7,8]. Gel electrolyte systems commonly have poor mechanical strength and low electrochemical stability. Additionally, the crystalline areas of the polymer matrix are also disadvantageous for the gelation process, as it results in poor ionic transport [9]. Therefore, a novel gel polymer electrolyte with improved electrochemical and physical properties is demanded in order to implement its practical application.

Significant efforts have been expended in recent years to address the aforementioned problems. Different polymer matrices with polar functional groups have been considered for preparing GPEs such as poly (ethylene oxide) (PEO) [10], poly (vinyl alcohol) (PVA) [11], poly (methyl methacrylate (PMMA)) [12], poly (acrylonitrile) (PAN) [13], poly (vinylidene fluoride) (PVDF) [14], and co-polymer poly (vinylidene fluoride-hexafluoro propylene) (P(VDF-HFP)) [15]. Among those PVA is a very attractive polymer for GPE fabrication due to its excellent solvent holding capacity, good film-forming capability, biodegradability, and low toxicity [16]. Also, PVA is a water-soluble polymer, therefore it avoids using aggressive and toxic solvents such as acetone, 1-methyl-2--pyrrolidinone (NMP), or dimethylformamide (DMF) during preparation of the material. Besides, it has a wide range of temperatures where it remains in the stable gel phase. However, the pure PVA doesn't have sufficient mechanical and thermal stability to be applied as a polymer matrix for GPEs [17]. In order to improve these characteristics of PVA-based polymer matrix a variety of methods have been adopted including blending with other polymers [18], cross-linking [19], and insertion of ceramic fillers [20]. Lin Guo et al. prepared hydrogel electrolyte by chemical cross-linking of polyvinyl alcohol and polyethylene glycol (PEG) with glutaraldehyde (GA), which showed improved mechanical properties and ionic conductivity compared to pure PVA hydrogel [21]. Wang and co-authors also reported the enhancement of mechanical characteristics and liquid absorption properties of the PVA-based gel electrolyte by crosslinking with GA [19]. The introduction of chemically cross-linked bonds into the structure of the host polymer is considered as an effective way of enhancing the mechanical properties, thermal and dimensional stability of GPEs, as well as reducing the crystallinity of the polymer. In addition to the mechanical stability, good liquid absorbency is important to develop a membrane with smooth ion conduction channels and high ionic conductivity [17]. Therefore, the membranes with nanofibrous structures with their large specific surface area, high porosity, and interconnected void structure were introduced recently, which facilitate the electrolyte solution absorption and retention [22]. Electrospinning technology is the foremost method of homogenous and continuous nanofiber production from polymer solutions with a numerous advantages such as low cost, easy operation, and a wide range of spinning precursors [23].

There are only a few works reported on PVA-based nanofibrous GPE for LIBs. One of them is the PVA-based composite nanofiber GPE with TiO_2 particles by Morshed et al. which provided a large surface area, high porosity, and electrolyte uptake [17]. Sui et al. fabricated soy protein isolate (SPI)/poly(vinyl alcohol) (PVA) composite GPE nanofiber membrane with green chemical technology, where the interfacial resistance was reduced compared to pure PVA membrane [24]. However, the ionic conductivity of those electrolytes is quite low (1–2.5 $\times$ 10^{-5} S cm^{-1}) for application in LIBs. Nevertheless, the further development of PVA-based composite materials using electrospinning technique and combining them with functionalized polymers and additives (inorganic, hybrid compounds) is a very promising way to eliminate the disadvantages associated with poor electrochemical and mechanical properties.

Here, we introduce a novel, dual crosslinked nanofiber membrane (DCNM) made up of PVA, maleated PVA (PVA-MA) and tetraethyl orthosilicate (TEOS) to apply as GPE for LIBs after activating with liquid electrolyte. The photocrosslinking reaction of photosensitive PVA-MA and polyethylene glycol diacrylate (PEGDA) occurred simultaneously during the electrospinning process by UV-irradiation. Nanofiber membranes were additionally crosslinked by sol-gel crosslinking through Si–OH groups via thermal treatment. The crosslinking between TEOS and PVA significantly enhanced mechanical strength of the membrane as well as its flexibility after swelling with liquid electrolyte. The highest value of ionic conductivity was achieved for GPEs with 30 wt% of TEOS, 1.98 $\times$ 10^{-3}, which is significantly higher than that of a commercial separator Celgard2500 (0.36 $\times$ 10^{-3} S cm^{-1}) and pure PVDF based GPE (0.074 $\times$ 10^{-3} S cm^{-1}) [25]. The assembled lithium metal cell with this GPE showed outstanding electrochemical performance. A Li/GPPM/Li-$FePO_4$ exhibits excellent rate performance with specific discharge capacities of 153, 143, 130, 115, 101 and 80 mA h g^{-1} at 0.1, 0.2, 0.5, 1, 2, and 5 C, respectively. The cell delivers a high reversible capacity of 133 mA h g^{-1} at 0.1 C and retains 87% of the initial discharge capacity after 150 cycles. Proposed GPE system could efficaciously suppress the growth of Li dendrites during the long cycling in contrast to the commercial separator, and is a promising candidate for flexible LIBs.

2. Experimental

2.1. Materials

Polyvinyl alcohol (PVA, M_w = 146,000–186,000, 87–89% hydrolyzed), maleic anhydride (MA), tetraethyl orthosilicate (TEOS), polyethylene glycol diacrylate (PEGDA, M_n = 575), Triton X-100, p-toluene sulfonic acid, 2-hydroxy-2-methyl-1-phenyl-1-propan-1-one (Darocur® 1173) were purchased from Sigma Aldrich (Netherlands). Materials for LIB tests: Al foil (~20 mm), Li metal foil (>99.9%), $LiFePO_4$ powder, acetylene black (AB, MTI Co., Richmond, USA), poly(vinylidene fluoride) (PVdF, Kynar, HSV900, Richmond, USA), N-methyl-2-pyrrolidone (NMP, >99.5% purity, Sigma-Aldrich, Netherlands) and LiTFSI (bis (trifluoromethane)sulfonimide) salts (1 M concentration) in 1:1 mixtures of the organic solvents 1,2-dimethoxyethane (DME) and 1,3-dioxolane (DOL). Commercial microporous monolayer membrane (Celgard 2400) was purchased from Celgard LLC, USA.

2.2. Preparation of spinning solution

2.2.1. PVA modification with MA

The modification of terminal groups of PVA with MA was done according to the literature [26]. The maleated polyvinyl alcohol copolymer (PVA-MA) was synthesized by mixing 8 wt% PVA aqueous solution with maleic anhydride (MA) at mass ratio of 9:1 respectively. The mixture was stirred at 70 °C for 3 h and let cool down to room temperature.

2.2.2. TEOS pre-hydrolysis

Pre-hydrolysis reaction of TEOS was carried out by following procedure in the literature [27]. 3 g (14 mmol) TEOS and 0.77 g (42 mmol) water were mixed homogeneously in 1.33 mL ethanol. After adding 0.05 g of p-toluene sulfonic acid (catalyst), the mixture was stirred at 5 °C for 2 h and further left overnight at room temperature. The

water/silicone ratio is calculated as r = 3.

2.3. Electrospinning/nanofiber fabrication and preparation of GPE

The spinning solution was prepared by mixing 10 wt% PVA aqueous solution with PVA-MA solution in different weight ratios 9:1, 8:2, 5:5 respectively. Further, pre-hydrolyzed TEOS, PEGDA as a crosslinker and Triton X-100 as a surfactant were added to the mixture and sonicated in an ultrasonic bath for 40 min. The formulations of the spinning solution are given in Table 1. The dual crosslinked nanofiber membrane (DCNM) was fabricated by electrospinning technique with simultaneous irradiation by the UV lamp (Spectroline, ENF-240C/FE, $\lambda_{max} = 365$ nm). The processing condition is taken with an applied voltage of 20 kV, a flying distance of 15 cm, and a solution feeding rate of 0.9 mL h^{-1}. Nanofibers were collected on a rotating drum covered with Al foil with a rotation speed of 100 rpm. Final membrane was dried in a vacuum oven at 60 °C overnight.

DCNMs were punched into small discs with a diameter of 19 mm and GPEs were obtained by immersing into liquid electrolyte (1 M LiTFSI in DOL/DME 1:1 v/v) for 1 h in the glove box. The nanofibrous GPEs were used after removal of excess liquid electrolyte with a filter paper to investigate electrochemical properties.

2.4. Characterization

The surface microstructure and morphology of the membranes were observed by scanning electron microscopy (SEM, EDX ZEISS Crossbeam 540, Germany). Samples for SEM analysis were coated with gold by an Automatic sputter coater (Q150T, Japan) to reduce charging. The structure of the prepared fibers was observed by transmission electron microscopy (TEM, JEOL JEM - 1400 Plus, USA). The accelerated voltage of TEM was 120 kV. The materials' structure and chemical composition were analysed by Fourier transform infrared spectroscopy (FTIR, Thermo Scientific Nicolet iS10 FT-IR Spectrometer, USA) with a wavenumber range of 4000–400 cm^{-1}. The thermal stability of the fibrous membranes was tested by thermogravimetric analysis (TGA, STA 6000, Perkin Elmer, USA) and measurements were carried out from 20 to 600 °C at a rate of 20 °C min^{-1} under a dry nitrogen atmosphere. Differential scanning calorimetry (DSC) measurements of polymer membranes was carried out at a heating rate of 10 °C min^{-1} under nitrogen atmosphere on the Perkin Elmer Diamond DSC instrument.

The electrolyte uptake (A) of nanofibrous membranes was determined by immersing the membranes into liquid electrolyte for 1 h, and calculated by the following equation:

$$A(\%) = \frac{W_2 - W_1}{W_1 * 100\%}$$

where W_1 and W_2 were the weight of dry and wet membranes, respectively.

Table 1
Formulations of DCNM and its average fiber diameters (AFD).

Polymer membranes	PVA solution (10 wt%.)	PVA-MA	PEGDA	TEOS	AFD, nm
PPM1	90.0	9.0	1.0	0	350
PPM1-T1	81.0	8.1	0.9	10.0	470
PPM1-T2	72.0	7.2	0.8	20.0	734
PPM1-T3	63.0	6.3	0.7	30.0	910
PPM2	80.0	18.0	2.0	0	370
PPM2-T1	72.0	16.2	1.8	10.0	524
PPM2-T2	64.0	14.4	1.6	20.0	744
PPM2-T3	56.0	12.6	1.4	30.0	949
PPM5	50.0	45.0	5.0	0	464
PPM5-T1	45.0	40.5	4.5	10.0	560
PPM5-T2	40.0	36.0	4.0	20.0	712
PPM5-T3	35.0	31.5	3.5	30.0	954

Gel fraction (GF) was determined by immersing the tested samples (d = 16 mm) in DMC (20 mL) at room temperature for 24 h. After removing solvent residue gently, the sample was dried in a vacuum oven at 60 °C overnight. Gel fraction is calculated from the following equation:

$$GF\ (\%) = \frac{W_{\text{remained}}}{W_{\text{total}}} \times 100\%$$

where W_{total} and $W_{remained}$ is sample weight recorded before and after the test.

Porosity (P) was measured by weighting the mass difference of sample before and after being immersed into n-butanol at room temperature. Excess n-butanol was gently wiped off by tissue. Porosity was derived from the following equation:

$$P\ (\%) = \frac{M_{BuOH}/\rho_{BuOH}}{M_{BuOH}/\rho_{BuOH} + M_p/\rho_p} \times 100$$

where M_p is the weight of dry sample, M_{BuOH} is weight of sample absorbed solvent, and ρ_p, ρ_{BuOH} are densities of the polymer and the used solvent, respectively.

The ability of the membrane to hold the absorbed electrolyte over a period of time is defined in terms of the relative absorption ratio R_A. It was measured by soaking the membrane into electrolyte for 4 h to reach saturation and then recording the weight changes of the swollen membrane kept under standard load as a function of time. The parameter, R_A is then calculated as:

$$R_A = \frac{M_{PE}}{M_{\text{PE, saturated}}}$$

where $M_{PE,saturated}$ is the mass of the PE when the membrane is fully saturated with the electrolyte and M_{PE} that of the PE after a time interval when the saturated PE has been squeezed by pressing it under load of 5 N.

The *mechanical strength* of fibrous membranes was characterized by a tensile tester (Materials Testing Machine Z010/TN2S). The tensile rate was set as 10 mm min^{-1}, and each sample was cut into the size of 10 mm × 50 mm for the measurement. The tensile strength δ_t and broken elongation ε_t were calculated according to equations:

$$\delta_t = \frac{P}{bd}$$

$$\varepsilon_t = \frac{L - L_0}{L_0} \times 100$$

where P is the load, b is the width of the sample, d is the thickness of sample, L is the length of sample when fractured, and L_0 is the initial length of the sample.

2.5. Electrochemical characterization

The ionic conductivity was determined by electrical impedance spectroscopy (EIS) in the range of 0.1 Hz − 1 MHz using a coin type cell with GPE sandwiched between stainless steel (SS) blocking electrodes. The ionic conductivity was determined according to the following equation:

$$\sigma = \frac{h}{R_b S}$$

In this equation, σ is the ionic conductivity, R_b represents the bulk resistance of the membrane, h is the thickness, and S is the area. The electrochemical stability was studied by linear sweep voltammetry (LSV) assembling CR2032 coin cell, with stainless steel as a working, and Li metal as a reference electrode. The potential voltage range was from 2.0 V to 6.0 V at a scan rate of 0.1 mV s^{-1} at room temperature. LSV and EIS measurements were performed on a VMP-3 potentiostat/galvanostat

(Bio-Logic Instruments, France). Galvanostatic Li plating/stripping cycling tests were also performed on a VMP-3 potentiostat/galvanostat at a current density of 0.5 mA cm^{-2} to investigate the formation and growth of the Li dendrites in the symmetric Li/Li cells with the prepared GPEs and liquid electrolyte (LE). Li/GPE/Li and Li/LE/Li coin cells after 125 cycles of stripping/plating were disassembled in argon filled glove box to analyze the surface morphology of the lithium electrodes after cycling. In order to investigate the electrochemical performance of the GPEs, the CR2032 coin-type cells were assembled by using $LiFePO_4$ and Li foil in an argon-filled argon filled glove box (MasterLab, MBraun, Germany) as positive and negative electrodes, respectively. The charge and discharge test of assembled cells was carried out on a multichannel battery tester (BT-2000, Arbin Instruments Inc., TX, USA) with a voltage range of 2.5–4.2 V. The positive electrode was prepared by mixing the commercial $LiFePO_4$, acetylene black and PVDF in N-methyl-pyrrolidinone (NMP) solution in a weight ratio of 85:10:5. The slurry was casted by a doctor blade on a carbon coated aluminum foil and dried at 60 °C in a vacuum oven to remove the solvent. Further, the electrode was cut into disks (14 mm in diameter) and stored in an Ar filled glove box prior to use.

3. Results and discussion

Dual crosslinked nanofibrous membranes (DCNM) were fabricated from the solution of PVA, maleated PVA (PVA-MA), polyethylene glycol diacrylate (PEGDA) and tetraethyl orthosilicate (TEOS) by UV-electrospinning technique. Prior to preparing the spinning solution PVA-MA was obtained through esterification reaction in aqueous solution (Fig. 1a) and its chemical structure was investigated by FTIR spectroscopy. As shown in FTIR spectra in Fig. 1c, broad strong peaks at 3270 cm^{-1} (–OH stretching), 2940 cm^{-1} (asymmetric stretching of CH_2) and 1320-1325 cm^{-1} C–H deformation vibration (–CH stretching), 1636 cm^{-1} (due to water absorption, C═O carbonyl stretch), 1420 cm^{-1} (–CH bending) (C–H bending vibration of CH_2), and 1250, 1095 cm^{-1} (–C–O stretching) are characteristic peaks of pristine PVA [28]. The peaks of PVA-MA at 1740 and 1240 cm^{-1}, shifted in comparison with pure PVA, represent C═O and C–O stretching, respectively, which indicates the interactions between PVA and MA [29]. The ester linkage between PVA and MA is confirmed by a novel peak at 1178 cm^{-1} (Fig. 1c).

The pre-hydrolysis of TEOS was carried out further to form a sol and a gel in electrospinning precursor solution by a condensation reaction (Fig. 1b). It can be seen that after hydrolysis a broad absorption peak at 3278 cm^{-1} appears due to the formation of Si–OH bond (Fig. 1 d).

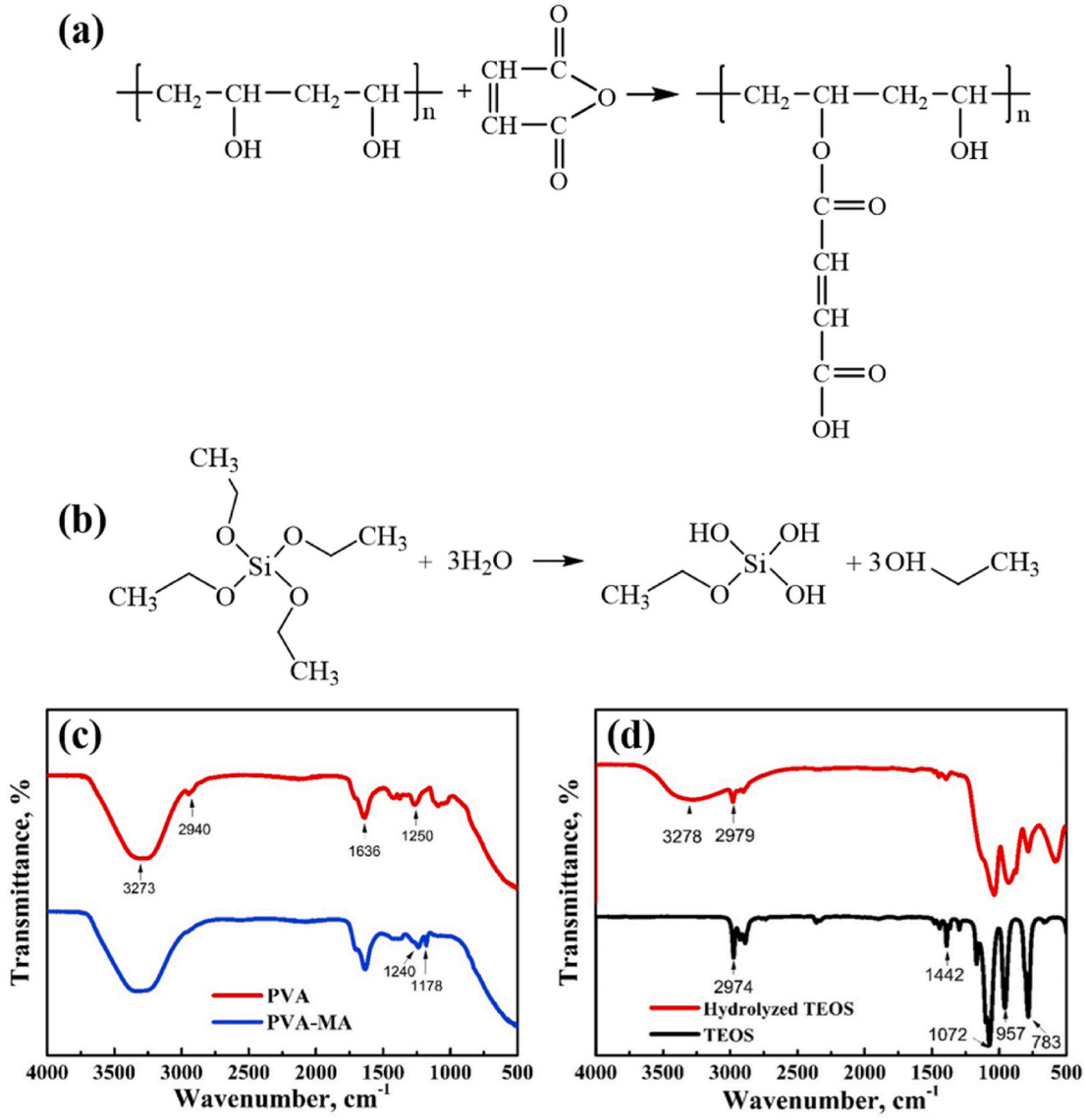

Fig. 1. Reaction scheme of (a) PVA maleation and (b) TEOS hydrolyzation; FT-IR spectra of (c) PVA solution and maleated PVA, (d) TEOS and hydrolyzed TEOS.

Furthermore, DCNM were fabricated with electrospinning technique and UV-irradiation at the same time as schematically illustrated in the Fig. 2. The dual crosslinking reactions occurred between photosensitive PVA-MA and PEGDA by UV-photocrosslinking, as well as between PVA and TEOS through Si–OH groups by sol-gel process during thermal treatment (Fig. 3a). The ratio of PVA-MA, PEGDA, and TEOS in the PVA-based membrane was varied in order to fabricate a membrane with high stability in organic liquid electrolyte solvents, and improved physical and electrochemical properties (Table 1). The FTIR spectra of the final membrane is given in Fig. 3b. The peak at 1635 cm^{-1} of DCNM represents the acetate group coming from vinyl acetate, which is the initial monomer of partially hydrolyzed PVA (87–89% hydrolyzed). In fabricating the crosslinked membranes, the hydroxyl groups in the repeating units of PVA were expected to produce strong secondary interactions with these silanol groups to form hydrogen and covalent bonds. The broad bonds appeared at around 1085–1246 cm^{-1} due to the siloxane bonds (Si–O–Si) from subsequent condensation reactions of silanol groups of TEOS during membrane drying [29]. The high gel fraction of membranes also reveals that crosslinking has successfully occurred within PEGDA and PVA-MA as well. In addition, MA acts as an organic-inorganic coupling agent, improving the mechanical strength of the material.

Fig. 4 shows the surface morphology of electrospun polymer membranes. From SEM images, it can be seen that the fibers formed without any beads with smooth surface, and have diameters of about 350, 500, 700, 900 nm for PPM1, PPM1-T1, PPM1-T2, and PPM1-T3 membranes respectively. With the increase of TEOS content in the solution, the average diameter of nanofibers exhibited an ascending trend which might be attributed to the changes in viscosity, surface tension, and electrostatic repulsion of the spinning solution. The increase of fiber diameters with the increase of TEOS content has been noticed according to the results of TEM analysis as well (Fig. S2). Since the TEOS alone does not show a high viscosity, the crosslinking of PVA by the silanol groups of TEOS increases the viscosity of the spinning precursor solution by time and this also results in increase of final fiber diameters [30]. Moreover, there were no any particles observed from TEM images corresponding to inorganic Si/SiO_2 particles, which confirm the fabrication of uniform fibers with homogeneous composition. It is worth mentioning that in addition to the cylindrical shape, the fibers also exist in ribbon-shaped form. The formation of ribbon-shaped fibers was due to thick polymer jets ejected from Taylor cones on the electrode of free surface electrospinning and fast solvent evaporation rate caused by high solution conductivity. Hiroyuki Itoh et al. demonstrated that membranes with ribbon-shaped fibers show better mechanical properties than cylindrical shaped ones which is related to their different deformation behavior [31]. In addition, it is seen that the fibers interlaid and form a 3D networked space with interconnected pores/voids between the fibers. Such a structure is advantageous for easy penetration of liquid electrolyte into the membrane structure and prevention of leakage, resulting in high ionic conductivity and mechanical properties.

The enhanced thermal stability of the membranes provides the safety of the battery at high temperatures and greatly favors their application in LIBs. TGA analysis was conducted for the DCNMs in the temperature range of 25–600 °C under nitrogen atmosphere at a heating rate of 20 °C min^{-1}, and the thermogram profiles are given in Fig. 5a. The slight weight loss in all samples of about 3–4% below 150 °C was due to the moisture absorbed during the preparation and handling of the samples. It was observed that thermal stability improved with increase of TEOS content in the membranes PPM1<PPM1-T1<PPM1-T2<PPM1-T3. For PPM1-T1, PPM1-T2, PPM1-T3 membranes, both the decomposition temperature and the residual weight were found to be higher when compared with membranes without TEOS content (PPM1) due to the hybrid structure which contains siloxane bonds (Si–O–Si) [32]. In temperature ranges of 150–300 °C, the weight loss of the samples was about 10–15% which is related to the evaporation of bounded and unbounded water molecules in PVA and TEOS structure. DCNMs perform excellent thermal stability, as the main degradation starts from 300 °C, and they can be safely applied for LIBs.

According to DSC profiles (Fig. S1), PPM1 membrane showed glass transitions (T_g) around −1 °C, and T_g for PPM1-T1, PPM1-T2, PPM1-T3 were not observed which is typical phenomena for the crosslinked structures. There were no phase transition points observed for all samples, which indicates that crosslinked structure hindered the crystallization of the membranes. The amorphousness of DCNM is advantageous for facilitating Li^+ ion movement and enhancing ionic conductivity of the GPE system.

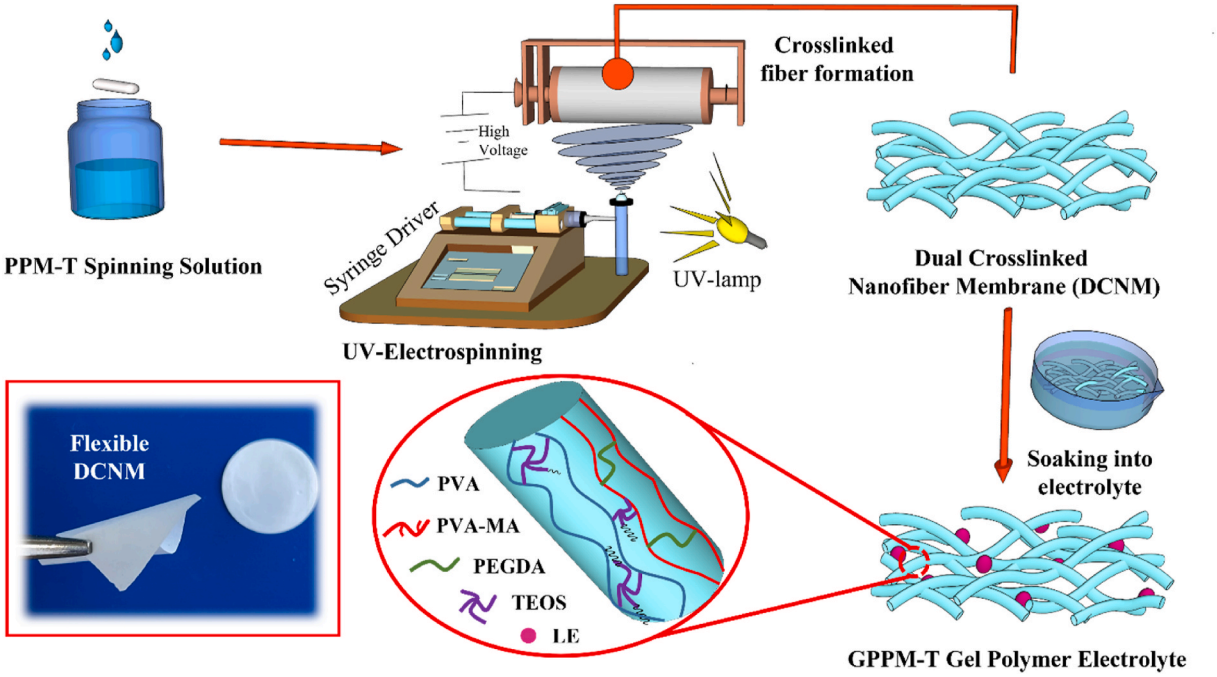

Fig. 2. Schematic illustration of dual crosslinked nanofiber membrane PVA/PVA-MA/TEOS (PPM-T) gel polymer electrolyte preparation by UV-electrospinning technique.

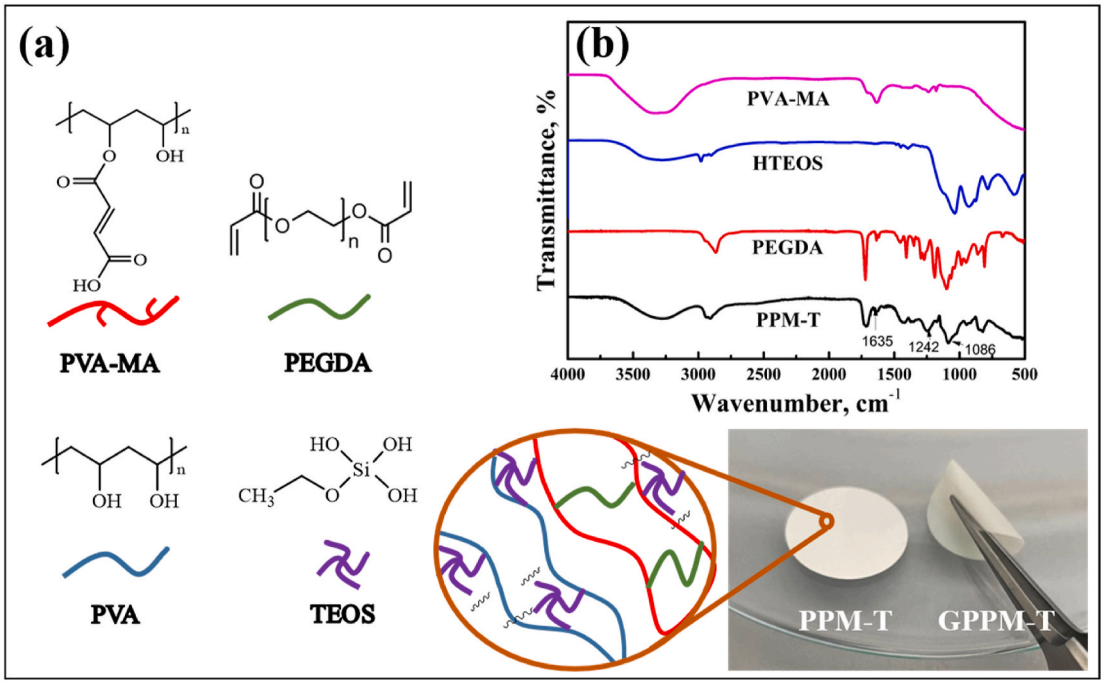

Fig. 3. (a) Composition and photo image (illustration) of the dry PPM-T membrane and GPPM-T gel electrolyte, and (b) FTIR spectra of DCNM.

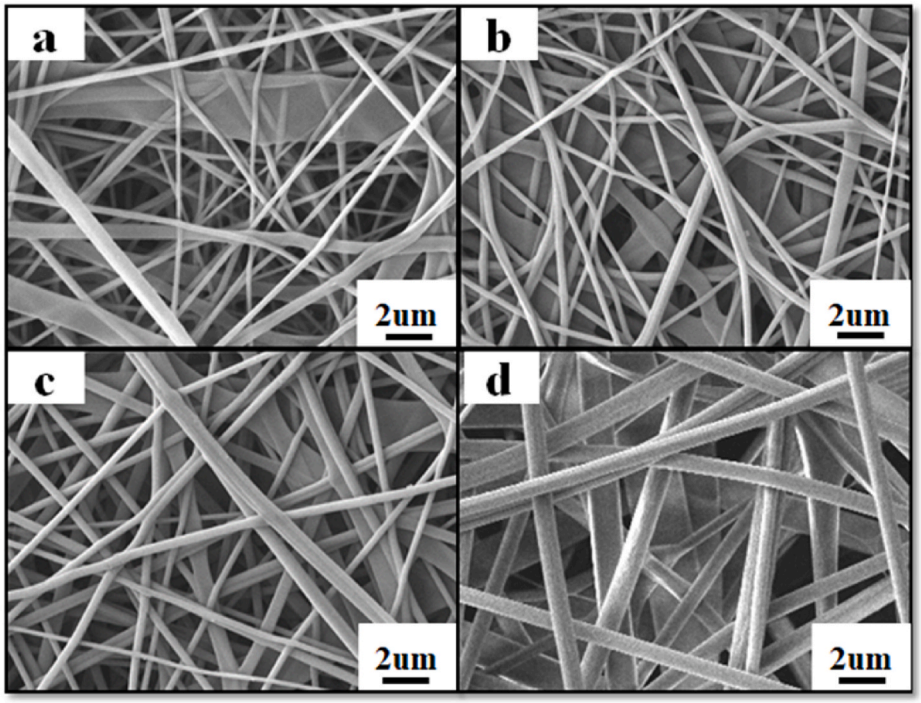

Fig. 4. SEM images of DCNMs: (a) PPM1; (b) PPM1-T1; (c) PPM1-T2; (d) PPM1-T3.

The chemical stability of DCNMs in the liquid electrolyte was checked by calculating gel fraction values. Nanofibrous membranes were immersed into organic solvent of liquid electrolytes, and after drying for 24 h, gel fraction values were calculated as explained in the Experimental Part. As given in Table 2, the chemical stability of DCNMs increases from 95.4% to 99.5% for PPM1 and PPM1-T3 membranes, respectively, due to the cross-linking after the condensation reaction of hydrolyzed TEOS with PVA. Additional crosslinking with TEOS helps to prevent the dissolution of the polymer matrix in organic solvents.

Interweaving structure of fibers is a beneficial feature of an electrospun membrane due to creation of a porous structure. At the same time, porosity is one of the important factors for polymer matrices for electrolytes. It facilitates penetration of liquid electrolyte into the membrane and helps to hold more liquid electrolyte providing an ion migration path to increase the ionic conductivity of polymer electrolyte. According to Table 2, porosity of the membranes increased with the rise of TEOS amount, and the highest porosity of 82.8% was determined for PPM1-T3 membrane. It directly affects another essential characteristic

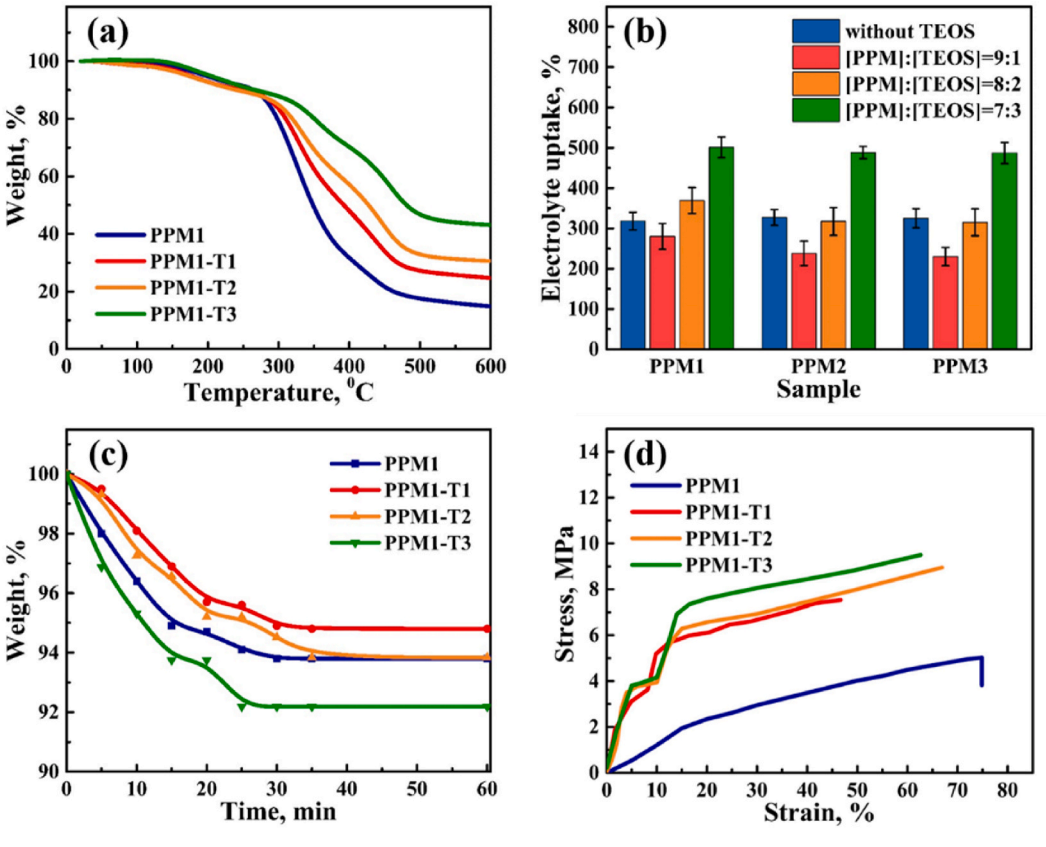

Fig. 5. (a) Thermo-gravimetric analysis (TGA), (b) liquid electrolyte uptake chart, (c) liquid electrolyte leakage tests results and (d) typical stress–strain curves of PPM1 membrane with different amount of TEOS.

Table 2
Main characterizations of DCNMs.

Polymer membranes	Gel fraction, %	Porosity, %	Electrolyte uptake, %	Conductivity, mS cm^{-1}
PPM1	95.4	75.5	318	0.68
PPM1-T1	97.4	74.2	280	0.55
PPM1-T2	98.7	81.7	369	1.76
PPM1-T3	99.5	82.8	501	1.98
PPM2	85.0	67.2	327	0.30
PPM2-T1	90.9	70.6	238	0.10
PPM2-T2	99.0	76.8	317	1.02
PPM2-T3	99.0	82.5	488	1.20
PPM5	77.6	67.7	325	0.12
PPM5-T1	79.7	65.0	230	0.09
PPM5-T2	89.8	81.5	315	0.64
PPM5-T3	96.8	81.9	487	0.65

of the membrane as electrolyte uptake, which also greatly depends on the chemical structure of the polymer matrix and the morphology of the materials. Fig. 5b showed the liquid electrolyte uptake value of PPM membranes with and without TEOS in the structure. It can be observed that all PPM membranes possessed a satisfying electrolyte uptake and the lowest value was 230%, which is still higher than that of some conventional matrices [33]. The maximum value reached 501% for PPM1 membranes with 30 wt% of TEOS. The high electrolyte uptake ability of DCNMs is attributed to the integrated effect of high porosity and interconnected voids between the fibers. High electrolyte uptake facilitates ion transportation efficiently, and is a critical property for the ionic conductivity of GPEs [34]. The 3D networked space with interconnected pores/voids between the fibers helps to easily penetrate liquid electrolytes into the membrane structure and avoid leakage. The experimental results for the electrolyte leakage behavior are shown in Fig. 5c. It can be seen that the leakage behavior of all PPM1 DCNMs reaches equilibrium within the first 30 min, and no leakage was observed thereafter. The crosslinked structure and hydrophilic nature of the PVA, and EO chains in PEGDA help to prevent leakage of the electrolyte solution; as a result, DCNMs exhibit a high liquid retention capacity. The crosslinked polymer membrane shows good compatibility with the electrolyte absorbing moderate amount of liquid electrolyte and at the same time retaining it within the structure due to the high affinity of PVA for the electrolyte solution. The maximum weight loss of 8 wt% was observed for PPM1-T3, which has the highest electrolyte uptake value. Compared to previously reported crosslinked membrane structures [22], all DCNMs showed significantly high liquid retention capacity.

The mechanical properties of GPE are very important not only for quality assurance during a rigorous manufacturing process, but also for proving the stability of GPE and suppressing the growth of lithium dendrites during charging and discharging cycles. The mechanical properties of crosslinked polymer films were evaluated by the results of standard tensile stress-strain tests summarized in Table S1. The Young's modulus values for PPM1 membranes with TEOS are much higher than without, which is expected due to crosslinked bonds in the structure. It leads to an improvement of the mechanical strength, however degreases the elongation at break of the samples. As it can be seen from the stress-strain curves of DCNMs presented in Fig. 5d, the tensile strength increased with the introduction of TEOS, which grew from 3.82 MPa to 7.54, 8.95 and 9.05 MPa for the PPM1, PPM1-T1, PPM1-T2 and PPM1-T3 membranes, respectively. This can be explained by the fact that the added TEOS are partially linked together with PVA based on condensation between hydroxyl groups in the PVA backbone and the hydroxyl in TEOS, and the appearance of crosslinking between TEOS chains after the condensation. However, strain was decreased due to the increased

brittleness of the polymer which associated with the high crosslinking degree of the membrane [35]. Meantime, it was shown in Fig. 3, that the GPEs can be fully bended after swelling in liquid electrolyte. All samples showed excellent mechanical stability which allowed to obtain membranes as thin as ~25 μm in a dry and ~30 μm in a gel form. Test on the mechanical properties makes it clear that the TEOS indeed leads to improving the tensile strength and GPE based on DCNMs can be safely used for flexible LIBs.

The ionic conductivity is the primary function of the electrolyte material, which remarkably influences the electrochemical performance of a whole battery. The conductivities of the DCNM GPEs were examined by electrochemical impedance spectroscopy (EIS) with stainless steel as blocking electrodes (SS/GPE/SS) at room temperature. The total resistance of the electrolytes consists of bulk resistance (R_b) and interfacial transition resistance. The impedance spectra of all GPE samples displayed similar plots, where R_b made the major devotion to the total impedance values (Fig. 6a). The ionic conductivity values of GPEs calculated from the impedance spectroscopy results are given in Table 2. The thickness of all GPEs were about ~30 μm, and were measured for each sample before assembling the coin cells. Addition of TEOS into the structure increased the conductivity values, which is attributed to the improved porosity, and high absorption of the liquid electrolyte resulting in enhanced ionic conductivity of the polymer electrolyte. The highest values were observed for PPM1, PPM2, and PPM5 membranes with 30 wt% of TEOS 1.98×10^{-3}, 1.20×10^{-3}, 0.65×10^{-3} S cm^{-1}, respectively. These results are much higher than that of the commercial separator Celgard2500 (0.36×10^{-3} S cm^{-1}) and pure PVDF membranes [25]. The formation of a stable solid electrolyte interface on the lithium metal electrode can conduct Li^+ freely and prevent dendrite generation deriving from any undesired interaction between the electrolyte components and lithium, which was essential for attaining good cycle performance [24]. Fig. 6 inset shows the initial interface impedance spectra of Li/GPE/Li cell containing GPPM1-T3 as a representative. As for typical GPEs, the semicircle at high-frequency region and straight linear line at the low-frequency region were observed. The interfacial resistance (R_i) of GPE can be seen from the diameter of the semicircle on the real axis called the charge-transfer resistance (R_{ct}) values [36]. The PPM1-T3 showed excellent stability with lithium electrodes, and R_i was 98 Ω which is far less than that of many reported GPE systems with similar dimensions [24,36,37].

It is known that the higher ionic conductivity of GPE compromises the mechanical strength of the membrane [38,39]. As discussed above the dual cross-linked structure of the developed GPEs allows to achieve high ionic conductivity along with sufficient mechanical strength. At the same time, a wide potential stability window of membranes is a crucial property to determine its application for high-voltage Li-metal batteries. Linear sweep voltammetry (LSV) was conducted to estimate the electrochemical potential stability window of the electrolytes using Li/GPE/SS cell configuration in a potential range from 2 to 6 V at 25 °C. Fig. 6b, shows the result for GPPM1-T3, which exhibits a stable potential window up to 5.1 V. There is no noticeable oxidation peak was observed up to 5.1 V, indicating that the GPPM1-T3 has sufficient electrochemical stability. In terms of ionic conductivity, thermal and mechanical stabilities all GPEs meet the basic requirement for gel electrolyte. As discussed above the increase of TEOS content significantly affects the ionic conductivity of GPE. Therefore, Li/GPE/$LiFePO_4$ cells were assembled with GPPM1 without TEOS and GPPM1-T3 with the highest TEOS content and electrochemical performance was evaluated. Initial charge–discharge properties of the cells with GPPM1 and GPPM1-T3 at 0.1 C rate (25 °C, 2.5–4.0 V) are shown in Fig. 7a. The unit cells showed flat charge and discharge potential plateaus at 3.48 and 3.38 V, respectively, which are typical properties of $LiFePO_4$ in the first cycle [40]. The cells exhibited initial discharge capacities of 147 and 153 mA h g^{-1} at 0.1 C for GPPM1 and GPPM1-T3, correspondingly. These values are around 90% of the theoretical capacity of $LiFePO_4$ (170 mA h g^{-1}). Notably, the cells perform small polarization (0.10 V), which is a promising result for gel-type electrolyte. The low polarization can be attributed to the excellent interface properties and high ionic conductivity.

The rate capabilities of the cells with GPE were investigated with stepwise varying charging currents from 0.1 C to 5 C every five cycles (Fig. 7b). Apparently, the Li/GPPM1-T3/LFP cell exhibits excellent rate performance with specific discharge capacities of 153, 143, 130, 115, 101 and 80 mA h g^{-1} at 0.1, 0.2, 0.5, 1, 2, and 5 C, respectively; while the cell with GPPM1 and Celgard exhibits notably lower capacity at higher C rates. Even going through 5 cycles with high current density of 5 C, the cell can still retrieve the high specific capacity of about 150 mA h g^{-1} when the current density decreased back to 0.1 C. Moreover, after 150 cycles, the relatively high discharge specific capacity of 124 and 133 mA h g^{-1} with the capacity retention rate of 87% still remains for the cells with GPPM1 and GPPM1-T3 GPEs (Fig. 7c). The better rate performances of the cells assembled with GPEs than Celgard can be correlated with higher ion conductivity, better affinity with the liquid electrolyte, and less formation of lithium dendrite on membrane surfaces resulting in faster lithium-ion transportation at high charge-discharge rates. The coulombic efficiency value close to 100% indicates high reversibility of the cell reactions and stable cycling performance. All these half-cell results emphasize that the electrolytes with higher TEOS content provides improved interface contact with electrodes and is a promising GPE system for flexible batteries.

At the same time, Fig. 7d also reveals that the gel polymer electrolyte can prevent the penetration of lithium dendrite and avoid the short circuit inside the battery effectively. The interfacial stability of GPE with Li metal was studied by galvanostatic Li plating/stripping measurements. For comparison, the symmetric cells with liquid and GPE

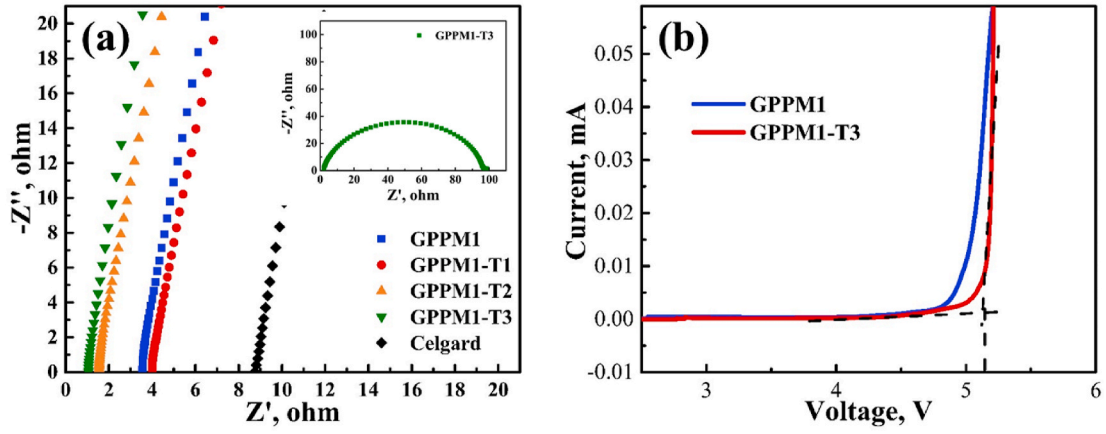

Fig. 6. (a) EIS spectra of SS/GPE/SS and SS/Celgard/SS symmetric cells and Li/GPPM1-T3/Li (inset); (b) Linear sweep voltammogram of Li/GPE/SS cells.

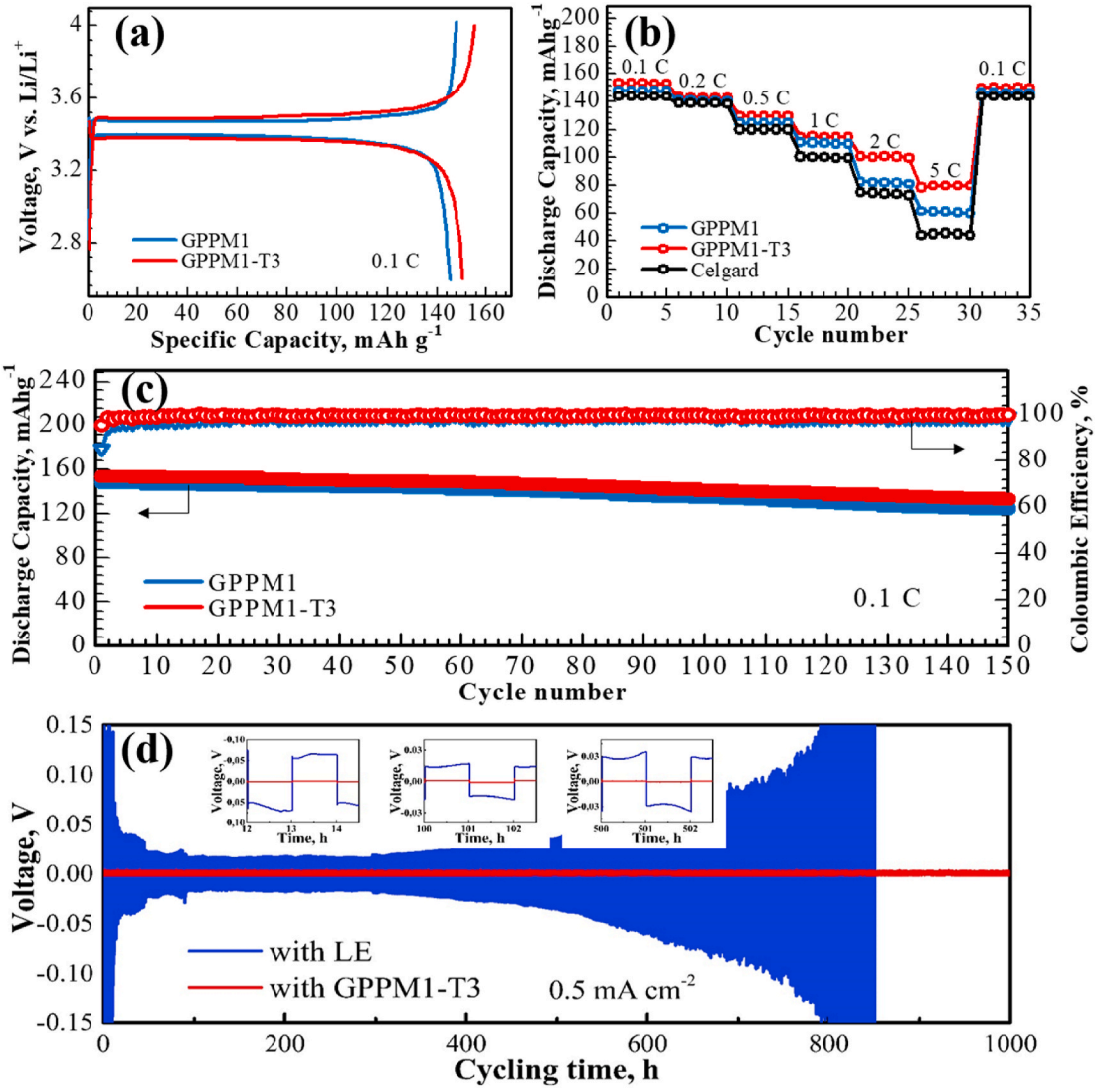

Fig. 7. (a) Initial charge-discharge profiles and (b) C rate performance; (c) Galvanostatic cyclability and Coulombic efficiency of Li/GPE/$LiFePO_4$ cells; (d) Galvanostatic cycling potential profiles for Li–Li symmetrical coin cell cycled at 0.5 mA cm^{-2} Celgard separator and GPE.

electrolytes, Li|LE|Li and Li|GPE|Li, were assembled and comparative electrochemical cycling tests of the electrolyte's compatibility with Li anode at a current density of 0.5 mA cm^{-2} were performed. The cell with LE showed polarization potential of around 150 mV in the initial 10 h and remained stable at 20 mV up to 300 h, which followed by gradual increase of potential. The increase of polarization is due to the Li dendrite formation and disturbance of the LE/Li interface leading to the complication of Li plating/stripping. The severe fluctuations with large potential hysteresis, imply the Li dendrite growth on the Li metal surface [41,42]. In contrast, the cell with GPE presented a considerably smaller polarization potential of 12 mV and remained stable for 1000 h, which indicates a remarkably improved interfacial and electrochemical stability in case of GPE and Li metal anode.

The surface morphology of the post-cycled Li electrode in the symmetric cell after 250 h of stripping/plating test was investigated by SEM analysis to observe Li dendrite growth. In comparison with the cell assembled with the liquid electrolyte, the cycled Li electrode with the GPEs showed smoother and more uniform surface morphology (Fig. 8b

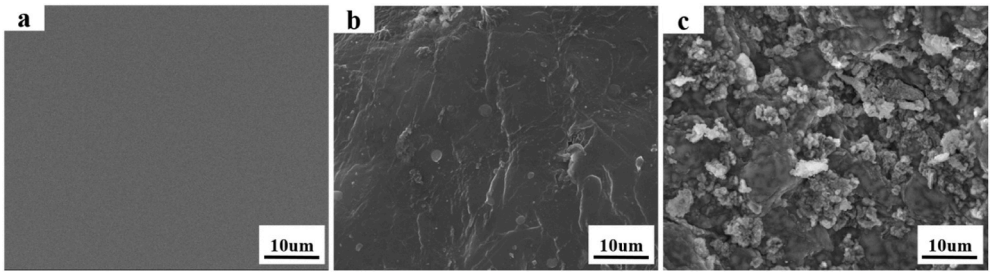

Fig. 8. The surface morphology of the (a) fresh Li electrode and Li electrode in the symmetric cell after 250 h of stripping/plating test with (b) GPPM1-T3 GPE and (c) liquid electrolyte at a current density of 1 mA cm^{-2}.

and c). Surface of the Li electrode electrochemically cycled within liquid electrolyte cell became porous and mossy which indicates the continuous formation of the lithium dendrites. The capability to immobilize the liquid electrolyte and a mechanical strength of the membrane inhibit the dendritic growth, which is beneficial to the cell performance [43].

4. Conclusion

In summary, a new dual crosslinked gel polymer electrolyte was proposed and fabricated by UV-electrospinning method. The structure design is advantageous for both the electrochemical and mechanical properties of the material. The membranes exhibit high porosity, electrolyte uptake, and liquid retention capacity and the crosslinked structure greatly enhances the thermal and mechanical stability of the obtained hybrid membranes. The highest value of ionic conductivity was achieved for GPPM1 GPEs with 30 wt% of TEOS 1.98×10^{-3}, which is much higher than that of the commercial separator Celgard2500 (0.36×10^{-3} S cm^{-1}) and pure PVDF based GPE [25]. Improvements in physical and electrochemical properties of DCNM were achieved owing to the interconnected voids between the fibers and crosslinked structure. In particular, crosslinking between TEOS and PVA affected the mechanical strength, porosity, and ionic conductivity of the membrane, while hydrophilic nature of PVA and ethoxy chains of PEGDA enhanced the liquid retention capacity. As a result, assembled half-cell battery with GPPM1-T3 showed improved interface contact with electrodes and exhibited high discharge specific capacity of 133 mA h g^{-1} with the capacity retention rate of 87% at 0.1 C. In addition, GPE system could efficaciously suppress the growth of Li dendrites during the long cycling in contrast to the commercial separator. These results indicate that developed DCNM is a promising matrix for GPE system to apply for flexible batteries.

CRediT authorship contribution statement

Nazym Kassenova: Conceptualization, Investigation, Methodology, Visualization, Writing – original draft, Writing – review & editing. **Sandugash Kalybekkyzy:** Conceptualization, Investigation, Methodology, Visualization, Writing – original draft, Writing – review & editing. **Memet Vezir Kahraman:** Conceptualization, Supervision, Writing – review & editing, Funding acquisition. **Almagul Mentbayeva:** Conceptualization, Supervision, Methodology, Resources, Writing – original draft, Writing – review & editing. **Zhumabay Bakenov:** Conceptualization, Supervision, Writing – review & editing, Funding acquisition.

Declaration of competing interest

The authors declare that they have no known competing financial interests or personal relationships that could have appeared to influence the work reported in this paper.

Acknowledgements

This work was supported by the research grants #51763/ПЦФ-МЦРОАП РК-19 ″New materials and devices for defense and aerospace applications” from Ministry of Digital Development, Innovation and Aerospace Industry of the Republic of Kazakhstan and AP09057868 “High performance polymer-based anion exchange membranes for alkaline fuel cells” projects from Ministry of Education and Science of the Republic of Kazakhstan. The authors wish to express their sincere thanks to Burcu Oktay from Marmara University for generous help with performing DSC and mechanical analysis, and Core Facilities of Nazarbayev University for providing services to use equipment and analyze the samples.

Appendix A. Supplementary data

Supplementary data to this article can be found online at https://doi.org/10.1016/j.jpowsour.2021.230896.

References

[1] A. Manthiram, An outlook on lithium ion battery technology, ACS Cent. Sci. 3 (2017) 1063–1069, https://doi.org/10.1021/acscentsci.7b00288.
[2] Y.G. Cho, C. Hwang, D.S. Cheong, Y.S. Kim, H.K. Song, Gel/solid polymer electrolytes characterized by in situ gelation or polymerization for electrochemical energy systems, Adv. Mater. 31 (2019) 1–12, https://doi.org/10.1002/adma.201804909.
[3] X. Zhang, S. Zhao, W. Fan, J. Wang, C. Li, Long cycling, thermal stable, dendrites free gel polymer electrolyte for flexible lithium metal batteries, Electrochim. Acta 301 (2019) 304–311, https://doi.org/10.1016/j.electacta.2019.01.156.
[4] M.W. Logan, S. Langevin, B. Tan, A.W. Freeman, C. Hoffman, D.B. Trigg, K. Gerasopoulos, UV-cured eutectic gel polymer electrolytes for safe and robust Li-ion batteries, J. Mater. Chem. A. 8 (2020) 8485–8495, https://doi.org/10.1039/d0ta01901a.
[5] N. Tolganbek, Y. Yerkinbekova, A. Khairullin, Z. Bakenov, K. Kanamura, A. Mentbayeva, Enhancing purity and ionic conductivity of NASICON-typed Li1.3Al0.3Ti1.7(PO4)3 solid electrolyte, Ceram. Int. 47 (2021) 18188–18195, https://doi.org/10.1016/j.ceramint.2021.03.137.
[6] S. Kalybekkyzy, A. Kopzhassar, M.V. Kahraman, A. Mentbayeva, Fabrication of UV-crosslinked flexible solid polymer electrolyte with PDMS for Li-Ion, Batteries 13 (2021) 1–12.
[7] M. Zhu, J. Wu, Y. Wang, M. Song, L. Long, S.H. Siyal, X. Yang, G. Sui, Recent advances in gel polymer electrolyte for high-performance lithium batteries, J. Energy Chem. 37 (2019) 126–142, https://doi.org/10.1016/j.jechem.2018.12.013.
[8] B. Liu, Y. Huang, H. Cao, L. Zhao, Y. Huang, A. Song, Y. Lin, X. Li, M. Wang, A novel porous gel polymer electrolyte based on poly(acrylonitrile-polyhedral oligomeric silsesquioxane) with high performances for lithium-ion batteries, J. Membr. Sci. 545 (2018) 140–149, https://doi.org/10.1016/j.memsci.2017.09.077.
[9] D. Zhou, D. Shanmukaraj, A. Tkacheva, M. Armand, G. Wang, Polymer electrolytes for lithium-based batteries: advances and prospects, Inside Chem. 5 (2019) 2326–2352, https://doi.org/10.1016/j.chempr.2019.05.009.
[10] M.A. Navarra, L. Lombardo, P. Bruni, L. Morelli, A. Tsurumaki, S. Panero, F. Croce, Gel polymer electrolytes based on silica-added poly(Ethylene oxide) electrospun membranes for lithium batteries, Membranes 8 (2018) 126.
[11] X. Ma, X. Huang, J. Gao, S. Zhang, Z. Deng, J. Suo, Compliant gel polymer electrolyte based on poly(methyl acrylate-co- acrylonitrile)/poly(vinyl alcohol) for flexible lithium-ion batteries, Electrochim. Acta 115 (2014) 216–222, https://doi.org/10.1016/j.electacta.2013.10.169.
[12] H.R. Jung, W.J. Lee, Electrochemical characteristics of electrospun poly(methyl methacrylate)/polyvinyl chloride as gel polymer electrolytes for lithium ion battery, Electrochim. Acta 58 (2011) 674–680, https://doi.org/10.1016/j.electacta.2011.10.015.
[13] K. Yang, X. Ma, K. Sun, Y. Liu, F. Chen, Electrospun octa(3-chloropropyl)-polyhedral oligomeric silsesquioxane-modified polyvinylidene fluoride/poly (acrylonitrile)/poly(methylmethacrylate) gel polymer electrolyte for high-performance lithium ion battery, J. Solid State Electrochem. 22 (2018) 441–452, https://doi.org/10.1007/s10008-017-3758-1.
[14] J. Xu, Y. Liu, Q. Cao, B. Jing, X. Wang, L. Tan, A high-performance gel polymer electrolyte based on poly(vinylidene fluoride)/thermoplastic polyurethane/poly (propylene carbonate) for lithium-ion batteries, J. Chem. Sci. 131 (2019) 49, https://doi.org/10.1007/s12039-019-1627-4.
[15] A. Aishova, A. Mentbayeva, B. Isakhov, D. Batyrbekuly, Y. Zhang, Z. Bakenov, Gel polymer electrolytes for lithium-sulfur batteries, Mater. Today Proc. 5 (2018) 22882–22888, https://doi.org/10.1016/j.matpr.2018.07.104.
[16] J. Lu, J. Gu, O. Hu, Y. Fu, D. Ye, X. Zhang, Y. Zheng, L. Hou, H. Liu, X. Jiang, Highly tough, freezing-tolerant, healable and thermoplastic starch/poly(vinyl alcohol) organohydrogels for flexible electronic devices, J. Mater. Chem. A. 9 (2021) 18406–18420.
[17] B. Zeytuncu, S. Akman, O. Yucel, M.V. Kahraman, Preparation and characterization of UV-cured hybrid polyvinyl alcohol nanofiber membranes by electrospinning, Mater. Res. 17 (2014) 565–569, https://doi.org/10.1002/aenm.201702561.
[18] F. Kingslin Mary Genova, S. Selvasekarapandian, N. Vijaya, S. Sivadevi, M. Premalatha, S. Karthikeyan, Lithium ion-conducting polymer electrolytes based on PVA–PAN doped with lithium triflate, Ionics 23 (2017) 2727–2734, https://doi.org/10.1007/s11581-017-2052-7.
[19] N. Lu, X. Zhang, R. Na, W. Ma, C. Zhang, Y. Luo, Y. Mu, S. Zhang, G. Wang, High performance electrospun Li+-functionalized sulfonated poly(ether ether ketone)/PVA based nanocomposite gel polymer electrolyte for solid-state electric double layer capacitors, J. Colloid Interface Sci. 534 (2019) 672–682, https://doi.org/10.1016/j.jcis.2018.09.027.
[20] V.R. Sunitha, S.K.M. Kabbur, G.S. Pavan, N. Sandesh, M.R. Suhas, C. Lalithnarayan, N. Laxman, S. Radhakrishnan, Lithium ion conduction in PVA-based polymer electrolyte system modified with combination of nanofillers, Ionics 26 (2020) 823–829, https://doi.org/10.1007/s11581-019-03225-9.

[21] L. Guo, W. Bin Ma, Y. Wang, X.Z. Song, J. Ma, X.D. Han, X.Y. Tao, L.T. Guo, H. L. Fan, Z.S. Liu, Y.B. Zhu, X.Y. Wei, A chemically crosslinked hydrogel electrolyte based all-in-one flexible supercapacitor with superior performance, J. Alloys Compd. 843 (2020) 155895, https://doi.org/10.1016/j.jallcom.2020.155895.
[22] Y. Tong, Y. Xu, D. Chen, Y. Xie, L. Chen, M. Que, Y. Hou, Deformable and flexible electrospun nanofiber-supported cross-linked gel polymer electrolyte membranes for high safety lithium-ion batteries, RSC Adv. 7 (2017) 22728–22734, https://doi.org/10.1039/c7ra00112f.
[23] S. Kalybekkyzy, A. Mentbayeva, Y. Yerkinbekova, N. Baikalov, M.V. Kahraman, Z. Bakenov, Electrospun 3D structured carbon current collector for Li/S batteries, Nanomaterials 10 (2020) 1–13, https://doi.org/10.3390/nano10040745.
[24] M. Zhu, C. Tan, Q. Fang, L. Gao, G. Sui, X. Yang, High performance and biodegradable skeleton material based on soy protein isolate for gel polymer electrolyte, ACS Sustain. Chem. Eng. 4 (2016) 4498–4505, https://doi.org/10.1021/acssuschemeng.6b01218.
[25] Q. Xiao, C. Deng, Q. Wang, Q. Zhang, Y. Yue, S. Ren, In situ cross-linked gel polymer electrolyte membranes with excellent thermal stability for lithium ion batteries, ACS Omega 4 (2019) 95–103, https://doi.org/10.1021/acsomega.8b02255.
[26] W. Sukhlaaied, S.A. Riyajan, Green synthesis and physical properties of poly(vinyl alcohol) maleated in an aqueous solutions, J. Polym. Environ. 22 (2014) 350–358, https://doi.org/10.1007/s10924-014-0651-1.
[27] M.V. Kahraman, N. Kayaman-Apohan, Z.S. Akdemir, Y. Boztoprak, A. Güngör, Synthesis of a novel bifunctional photoinitiator: hybrid coatings on polycarbonate, Macromol. Chem. Phys. 208 (2007) 1572–1581, https://doi.org/10.1002/macp.200700113.
[28] M.A. Abureesh, A.A. Oladipo, M. Gazi, Facile synthesis of glucose-sensitive chitosan–poly(vinyl alcohol) hydrogel: drug release optimization and swelling properties, Int. J. Biol. Macromol. 90 (2016) 75–80, https://doi.org/10.1016/j.ijbiomac.2015.10.001.
[29] Z. Xie, M. Hoang, T. Duong, D. Ng, B. Dao, S. Gray, Sol–gel derived poly(vinyl alcohol)/maleic acid/silica hybrid membrane for desalination by pervaporation, J. Membr. Sci. 383 (2011) 96–103, https://doi.org/10.1016/j.memsci.2011.08.036.
[30] T. Pirzada, S.A. Arvidson, C.D. Saquing, S.S. Shah, S.A. Khan, Hybrid silica – PVA nanofibers via sol – gel electrospinning, Langmuir 28 (2012) 5834–5844.
[31] H. Itoh, Y. Li, K.H.K. Chan, M. Kotaki, Morphology and mechanical properties of PVA nanofibers spun by free surface electrospinning, Polym. Bull. 73 (2016) 2761–2777, https://doi.org/10.1007/s00289-016-1620-8.
[32] J. Ma, M. Zhang, L. Lu, X. Yin, J. Chen, Z. Jiang, Intensifying esterification reaction between lactic acid and ethanol by pervaporation dehydration using chitosan-TEOS hybrid membranes, Chem. Eng. J. 155 (2009) 800–809, https://doi.org/10.1016/j.cej.2009.07.044.
[33] L. Zhao, J. Fu, Z. Du, X. Jia, Y. Qu, F. Yu, J. Du, Y. Chen, High-strength and flexible cellulose/PEG based gel polymer electrolyte with high performance for lithium ion batteries, J. Membr. Sci. 593 (2020) 117428, https://doi.org/10.1016/j.memsci.2019.117428.
[34] Z. He, Q. Cao, B. Jing, X. Wang, Y. Deng, Gel electrolytes based on poly (vinylidenefluoride-co-hexafluoropropylene)/thermoplastic polyurethane/poly (methyl methacrylate) with in situ SiO2 for polymer lithium batteries, RSC Adv. 7 (2017) 3240–3248, https://doi.org/10.1039/c6ra25062a.
[35] J. Wang, H. Bin Yao, D. He, C.L. Zhang, S.H. Yu, Facile fabrication of gold nanoparticles-poly(vinyl alcohol) electrospun water-stable nanofibrous mats: efficient substrate materials for biosensors, ACS Appl. Mater. Interfaces 4 (2012) 1963–1971, https://doi.org/10.1021/am300391j.
[36] M. Zhu, J. Wu, W.H. Zhong, J. Lan, G. Sui, X. Yang, A biobased composite gel polymer electrolyte with functions of lithium dendrites suppressing and manganese ions trapping, Adv. Energy Mater. 8 (2018) 1–10, https://doi.org/10.1002/aenm.201702561.
[37] K. Luo, D. Shao, L. Yang, L. Liu, X. Chen, C. Zou, D. Wang, Z. Luo, X. Wang, Semi-interpenetrating gel polymer electrolyte based on PVDF-HFP for lithium ion batteries, J. Appl. Polym. Sci. 138 (2021) 49993.
[38] Y. Liu, X. Ma, K. Sun, K. Yang, F. Chen, Preparation and characterization of gel polymer electrolyte based on electrospun polyhedral oligomeric silsesquioxane-poly(methyl methacrylate)8/polyvinylidene fluoride hybrid nanofiber membranes for lithium-ion batteries, J. Solid State Electrochem. 22 (2018) 581–590, https://doi.org/10.1007/s10008-017-3761-6.
[39] W. Ren, C. Ding, X. Fu, Y. Huang, Advanced gel polymer electrolytes for safe and durable lithium metal batteries: challenges, strategies, and perspectives, Energy Storage Mater 34 (2021) 515–535, https://doi.org/10.1016/j.ensm.2020.10.018.
[40] H. Fan, C. Yang, X. Wang, L. Liu, Z. Wu, J. Luo, R. Liu, UV-curable PVdF-HFP-based gel electrolytes with semi-interpenetrating polymer network for dendrite-free Lithium metal batteries, J. Electroanal. Chem. 871 (2020) 114308, https://doi.org/10.1016/j.jelechem.2020.114308.
[41] S. Wang, L. Zhou, M.K. Tufail, L. Yang, P. Zhai, R. Chen, W. Yang, In-Situ synthesized Non-flammable gel polymer electrolyte enable highly safe and Dendrite-Free lithium metal batteries, Chem. Eng. J. 415 (2021) 128846, https://doi.org/10.1016/j.cej.2021.128846.
[42] L. Li, M. Wang, J. Wang, F. Ye, S. Wang, Y. Xu, J. Liu, G. Xu, Y. Zhang, Y. Zhang, C. Yan, N.V. Medhekar, M. Liu, Y. Zhang, Asymmetric gel polymer electrolyte with high lithium ion conductivity for dendrite-free lithium metal batteries, J. Mater. Chem. A. 8 (2020) 8033–8040, https://doi.org/10.1039/d0ta01883j.
[43] M. Liu, S. Zhang, G. Li, C. Wang, B. Li, M. Li, Y. Wang, H. Ming, Y. Wen, J. Qiu, J. Chen, P. Zhao, A cross-linked gel polymer electrolyte employing cellulose acetate matrix and layered boron nitride filler prepared via in situ thermal polymerization, J. Power Sources 484 (2021) 229235, https://doi.org/10.1016/j.jpowsour.2020.229235.